ROYAL
AERONAUTICAL
SOCIETY

REGULAR PAPER

Propeller control for takeoff of a heavily loaded coaxial compound helicopter

Y. Zhao[1], Y. Yuan[2], R. Chen[1,*] and X. Yan[3]

[1]National Key Laboratory of Rotorcraft Aeromechanics, Nanjing University of Aeronautics & Astronautics, Nanjing, China,
[2]College of Engineering, Swansea University, UK and [3]Zhejiang Lab, Hangzhou, China
*Corresponding author. Email: crlae@nuaa.edu.cn

Abstract

Although a coaxial compound helicopter can takeoff without propeller in the normal condition, the distance should be as short as possible for obstacle avoidance when the vehicle operates in a confined area with heavy loads. Therefore, a suitable propeller control is required to improve the takeoff performance while the total power consumption is no more than the available power. The path is predicted by applying trajectory optimisation. Several varying takeoff parameters, including attitude, liftoff speed and obstacle height, are considered for optimum global performance. Three path indicators are proposed. Apart from typical distance and pilot workload, path sensitivity is quantified based on deviation from takeoff parameter variation. Results indicated that low propeller thrust at hover and moderate allocation on the propeller through flight is recommended. The aircraft achieves significantly improved takeoff performance compared to flight with pure rotors while maintaining the maximum takeoff weight. The distance is shortened by 12.6%, and the longitudinal pilot workload is alleviated by 9.8% and 7.3% from mean and maximum power frequency aspects. Besides, the path is less sensitive to takeoff parameter variations, such as speed, altitude and height.

Nomenclature

a_L	level acceleration rate
a_∞	lift scope
C_T	rotor lift coefficient
f_G	ground effect factor
$G_{\delta\delta}$	signal power
$G_{\omega A}$	longitudinal power frequency
$G_{\omega c}$	collective power frequency
H_O	obstacle height, m
H_R	rotor hub distance from ground, m
J	cost function
K_{A2pp}	allocation between the rotor and propeller
K_G	ground effect modifying coefficient
$(p, q, r)^T$	angular rates along body axes, rad/s
P_T	total power required, kW
R	rotor radius, m
$S_{(\bullet)}$	sensitivity indices
T_L, T_I, T_N	quantities relevant to pilot biodynamic model
$(u, v, w)^T$	velocity components along body axes, m/s
U	control variables vector, s^{-1}
V_{cL}	critical liftoff speed, m/s
V_{LO}	liftoff speed, m/s

| X | states variables vector |
| $(X, Y, Z)^T$ | position to ground, m |

Greek symbols

γ	climb angle, rad
δ	stick movements vector
$\delta_A, \delta_B, \delta_c$	longitudinal, lateral, collective stick movements, %
δ_r, δ_{pp}	yaw, and propeller stick movements, %
λ	inflow ratio
μ	advancing ratio
σ	rotor solidity
ω_{co}	cutoff frequency
$(\Phi, \Theta, \Psi)^T$	rigid body Euler angles, rad
$\Theta_{\min}$	low attitude boundary during takeoff, rad

Subscripts

u	quantities regarding the upper rotor
l	quantities regarding the lower rotor
pp	quantities regarding the propeller

Abbreviations

HLD	heavily loaded
IGE	in-ground effect
TRFs	time-frequency representations

1.0 Introduction

The coaxial compound helicopter has been proposed as a concept for future rotorcraft [1, 2] due to its high-speed performance. To achieve the outstanding characteristics, the helicopter utilises an auxiliary propeller and a pair of rigid rotors [3]. The rigid advancing-blade-concept rotors produce high moments for control power [1], leading to low propulsive force. The propulsion for forward flight is provided by the propeller, which greatly offloads the rotors and improves flight attitude in high-speed flights [4].

Most propeller control strategies are designed for high-speed performance and manoeuvrability [3, 5–7]. In the coaxial compound helicopter XH-59A [8, 9], the thrust from the auxiliary propulsion was controlled by a cockpit twist grip and only for high-speed flight. The propeller pitch in S-97 Radier [10] was scheduled based on level attitude for maximum aerodynamic performance. The propeller indeed plays a significant role in high-speed flight. However, a suitable propeller control is also needed for takeoff. X2 Technology Demonstrator (X2TD) applied a zero-thrust control after takeoff tests with or without the propeller [4, 11]. However, all initial accelerations of the tests were completed by rotors. As a result, the propeller's advantage for low-speed takeoff is not fully exploited. The extra propulsion benefits the aircraft's acceleration [12], which is crucial when the vehicle is in a restricted area with heavy loads.

The takeoff itself is risky for a conventional helicopter. Transportation Safety Board of Canada reported 77 takeoff accidents from 2003 to 2012. Among them, collision with terrain was the predominant factor in the 11 fatal accidents [13]. The takeoff procedure is more tricky for the vehicle with heavy loads at a hostile area with rough terrain, high temperatures and high altitudes. With very little excess power, the only feasible way for the heavily loaded (HLD) helicopter is to perform a short takeoff using ground effect [14, 15], as shown in Fig. 1. In this event, the aircraft's capability and the pilot's obstacle-avoidance technique are crucial for aircraft safety [16]. Either early or delayed climb out might result in obstacle contact.

The takeoff is more complex for a coaxial compound helicopter, due to its rigid rotors and propeller. In level acceleration, a high nose down or long distance is inevitable for a pure-rotor takeoff, limited
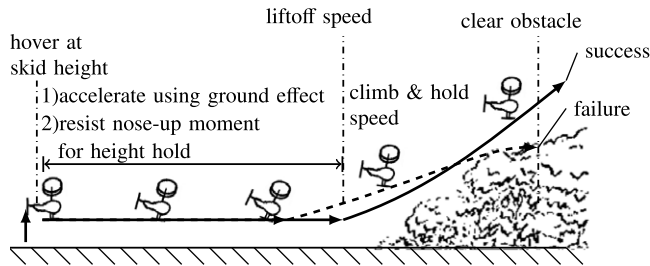
Figure 1. *Short takeoff procedure.*

by the low propulsion. As a result, it intensifies the risk of contact with ground or barriers. Aiming to ensure a safe takeoff procedure, the propeller could be utilised to provide additional propulsion [4, 12] for shorter distance. However, it aggravates the power deficiency in the heavily -loaded condition. Therefore, a propeller control strategy is required to strike a balance between airspeed acceleration and power cost to maximise aircraft's obstacle departure ability.

Most researches focus on pilot techniques for short takeoff distance. Schmitz [17, 18] optimised the HLD takeoff with a simple performance model. A two-phase linear path was proposed and was widely used as the nominal takeoff [15, 19, 20]. Enciu [16, 21] studied the speed for the shortest distance by simulation. Up-to-date, most research focus on predicting the climb phase while the acceleration phase was assumed to be constant. In addition, although takeoff distance is an important indicator, other factors, such as path sensitivities, are not considered in the technique development. Besides, no literature is relevant to engaging the propeller for the takeoff of a coaxial compound helicopter.

In light of discussions above, a propeller control strategy is designed to enhance the takeoff capability of a coaxial compound helicopter and ease of pilot operation. The propeller is engaged in hover and linked with the longitudinal stick. Takeoff paths are predicted by applying trajectory optimisation, where flight attitude, liftoff speed and obstacle height are varied in order to achieve a global optimum strategy. The performance is evaluated on the vehicle's capabilities and pilots' ease of implementation. Thus, three quantities are included: takeoff distance, pilot workload, and path sensitivities. Finally, the propeller control strategy is compared with the flight without the propeller.

2.0 Methodology

The research structure for the controller design is given in Fig. 2. Three key components are included: the flight dynamics model of the coaxial compound helicopter, takeoff path prediction and performance evaluation. In aircraft modelling, the longitudinal stick input is allocated to the propeller and rotors. Then trajectory optimisation is applied for takeoff path prediction, with certain cost function and path constraints. Finally, three performance quantities are used for evaluation.

2.1 Aircraft system modelling

The aircraft dynamics model consists of five parts: rotor system, propeller, fuselage, and two empennage surfaces. The rotor model's aerodynamic forces and moments are obtained based on the blade element method. The flapping motion of the rigid blade is simulated by applying the equivalent flapping offset and flapping spring method [2]. The complex inflow interference between coaxial rotors generates strong nose-up moments during low-speed flight [22]. Here, an analytical model with the first harmonic inflow approximation [8, 23] is applied.

The uniform inflows of coaxial rotors are calculated by revised momentum theory, that is,

$$
\begin{aligned}
f_{Gu}C_{Tu} &= 2v_{iu}\sqrt{\mu^2 + \lambda_u} \\
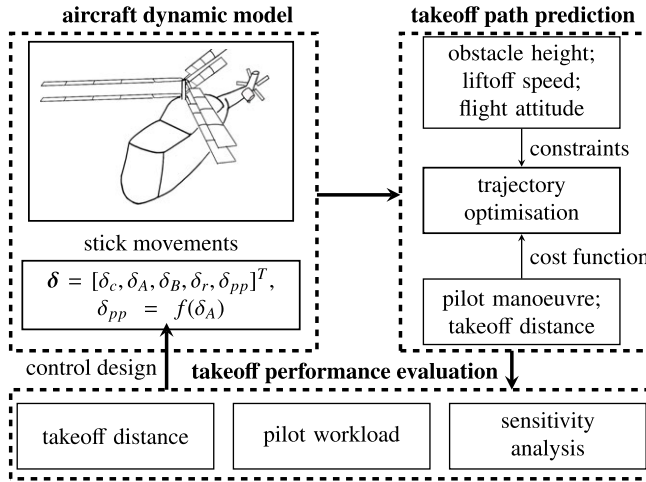f_{Gl}C_{Tl} &= 2v_{il}\sqrt{\mu^2 + \lambda_l}
\end{aligned}
\tag{1}
$$

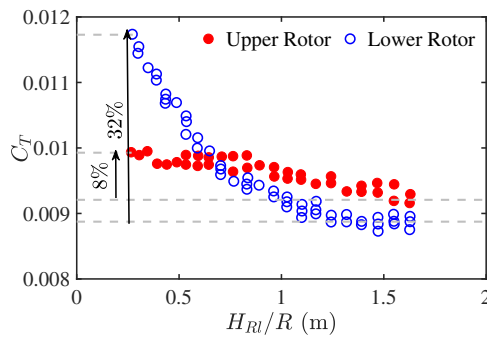**Figure 2.** *Structure of propeller control design for takeoff performance.*

Figure 3. *Ground effect of coaxial rotors in hover.*

where f_{Gu} and f_{Gl} are ground effect factors. The inflow λ_u and λ_l includes self-induced velocity and airflow interference approximated by rotor interference factors [24, 25]. Detailed descriptions of inflow calculation are given in Ref. (25).

Ground effect, increasing the rotor thrust when the helicopter is near the ground surface, is significant to the takeoff and landing performance. The "ground cushion" effect decreases the induced speed, i.e. decreases the induced power required. The influence of ground effect on power performance diminishes as the increase of flight altitude and flight. Cheeseman and Bennett [26] proposed the ground effect factor for the single rotor:

$$f_G = 1 - \frac{\sigma a_\infty \lambda}{4C_T} \frac{(R/4H_R)^2}{1 + (\mu/\lambda)^2} \tag{2}$$

Coaxial rotors have different ground effect factors due to mutual interference and different ground distances [27]. The measured data from Ref. (27), as shown in Fig. 3, indicates that the lower rotor has more thrust increment in the hover state. In contrast, the upper rotor is less sensitive to ground space changes, with only about 8% increment.

However, there is no quantified data on ground effect of the coaxial rotors regarding forward flight. Therefore, it is assumed that the trend of the coaxial rotors with speed is similar to that of a single rotor.

The ground effect of the coaxial rotors is simulated by modifying Equation (2) with coefficients K_{Gu} and K_{Gl}:

$$f_{Gu} = 1 - K_{Gu} \frac{\sigma a_\infty \lambda_u}{4C_{Tu}} \frac{(R/4H_{Ru})^2}{1 + (\mu/\lambda_u)^2}$$

$$f_{Gl} = 1 - K_{Gl} \frac{\sigma a_\infty \lambda_l}{4C_{Tl}} \frac{(R/4H_{Rl})^2}{1 + (\mu/\lambda_l)^2} \tag{3}$$

where K_{Gu} and K_{Gl} are fitted to meet the thrust increment at ground height of around $0.25R$ (shown in Fig. 3). They are set as 0.163 and 0.838 in this research, respectively. The coefficients are less than one due to the additional interference increasing the inflow ratio (λ_u and λ_l).

The modelling of the propeller is similar to that of the rotor, such as the aerodynamic loads and uniform induced inflow. Considering the propeller is controlled by a collective pitch, no flapping motion is simulated. A constant control allocation between the rotor longitudinal cyclic and propeller pitch is applied. Define coefficient K_{A2pp} as the ratio between their incremental stick input, that is,

$$K_{A2pp} = \frac{\Delta \delta_{pp}}{\Delta \delta_A} \tag{4}$$

Then their stick inputs are

$$\delta_A = \delta_{A0} + \Delta \delta_A$$

$$\delta_{pp} = \delta_{pp0} + K_{A2pp} \Delta \delta_A \tag{5}$$

where δ_{A0} and δ_{pp0} are determined by initial hover trim state.

The empennage surface aerodynamics is modelled with a lift-curve slope prior to stall and a general curve fit for large angles of attack. The fuselage aerodynamic loads are calculated using the scaled aerodynamic load coefficients [28, 29].

The flight dynamic model for the coaxial compound helicopter is expressed in the form of

$$\dot{X} = F(X, U, t) \tag{6}$$

where

$$\begin{cases} X = \begin{bmatrix} u & v & w & p & q & r & \Phi & \Theta & \Psi \\ X & Y & Z & \delta \end{bmatrix}^T \\ U = \dot{\delta} = [\dot{\delta}_c, \dot{\delta}_A, \dot{\delta}_B, \dot{\delta}_r, \dot{\delta}_{pp}]^T \end{cases}$$

where time derivatives of sticks $\dot{\delta}$ are introduced as control variables to avoid unreasonable discontinuities, also known as bang-bang control. In optimisation, numerical precision loss and error propagation might be caused by the multiple-magnitude variables. Hence, they are normalised and scaled to near unity to improve computational efficiency and rate of convergence, detailed can be found in Refs (25, 30).

A biodynamic model [31] considering pilot response delay is integrated into the dynamic model. After passing through the pilot biodynamic model, the pilot intentions are translated into actual control displacements in the cockpit, presented as

$$H_p(s) = \frac{T_L s + 1}{T_I s + 1} \frac{e^{-\tau_p s}}{T_N s + 1} \tag{7}$$

where $e^{-\tau_p s}$ is a pure time delay for pilot's cognitive responsiveness, $(T_L s - 1)/(T_I s + 1)$ reflects the lead/lag of pilot's control input, T_N is the neuromuscular lag time constant.
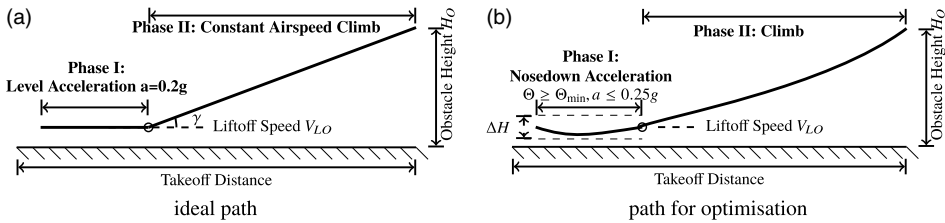
Figure 4. *Takeoff trajectory.*

2.2 Takeoff path prediction

The takeoff path prediction is transformed into a trajectory optimisation problem, which calculates the best operations and paths subjected to certain constraints. Details of the algorithm are given in Refs (30, 32). A short takeoff procedure consists of two stages: (1) level acceleration to liftoff velocity; (2) climb over a certain obstacle at height H_O, as shown in Fig. 4. The first subfigure presents the ideal takeoff, which is widely used as the nominal path [15, 16, 20, 33]. The helicopter first accelerates at a typical rate $0.2g$ [20] and holds constant height to accumulate kinetic energy for more excess power. After reaching liftoff speed, V_{LO}, the helicopter performs a climb out at angle γ (typically 6° [20]) and constant airspeed. Among all liftoff speeds, there is a critical speed, V_{cL}, for minimum takeoff distance to clear an obstacle.

The ideal path neglects the hover transition to acceleration and final climb out. In order to smooth the trajectory and improve the feasibility of the flight path, a height variation margin of ± 0.5m is applied to Phase I. The acceleration rate is below $0.25g$ considering the extra propulsion. Though decelerating velocity for fewer the takeoff distance is theoretically feasible in climbing, it is prohibited for ease of implementation [18]. No other constraint for the climbing angle or speed is included. According to take-off descriptions in Fig. 4(b), three flight parameters directly influence the takeoff: nose-down attitude, liftoff speed and obstacle height. The paths with varying parameters are considered for design a global optimum.

The cost function of the takeoff problem is described as

$$\min J = \frac{X_f}{X_g} + 0.1 \frac{t_f}{t_g} + \int_{t_0}^{t_f} \left(\dot{\delta}_c^2 + \dot{\delta}_A^2 + \dot{\delta}_B^2 + \dot{\delta}_r^2 \right) \mathrm{d}t \tag{8}$$

including (a) terminal distance and time, and (b) sum of the quadratic control derivations throughout the path. The distance and time are scaled by their estimated distance and time yielded from the ideal takeoff path, that is

$$X_g = \frac{V_{LO}^2}{2a_L} + \frac{H_O}{\tan \gamma} \tag{9a}$$

$$t_g = \frac{V_{LO}}{a_L} + \frac{H_O}{V_{LO} \tan \gamma} \tag{9b}$$

which helps improve the convergence speed and increases weight on control derivations for better handling quality.

To solve the nonlinear boundary value problem, a collocation method called direct multiple shooting [30, 34] is utilised. The problem is then transcribed into discrete nonlinear programming (NLP) by discretizing continuous states and controls into short time segments. Finally, the solution is obtained by solving NLP with the sequential quadratic programming method.
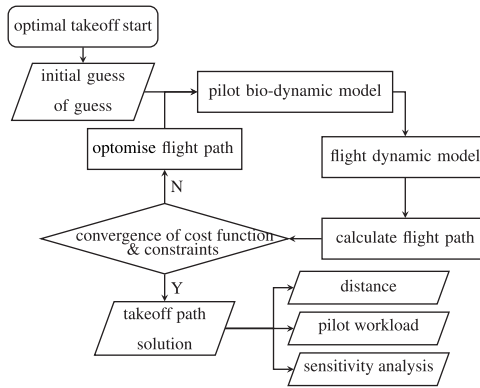
Figure 5. *Flow chart of takeoff path prediction and evaluation.*

2.3 Trajectory assessment

The minimum distance and stick variation rate are achieved through optimisation with certain constraints. Here, we aim to develop a global optimum propeller control. Hence, the paths and relevant manoeuvres with varying flight parameters are evaluated. The general layout of takeoff prediction and evaluation is presented in Fig. 5.

The takeoff distance, which is crucial for obstacle avoidance, is the most important indicator. It represents the capability of the aircraft. Besides, two quantities are applied to evaluate the ease of pilot implementation. One is pilot workload based on control inputs, and the other is path sensitivity to takeoff parameters.

2.3.1 Pilot workload evaluation

A helicopter's short takeoff significantly depends upon the pilot's control commands [21]. Although a minimum sum of the quadratic control derivations is achieved, the inherent workload of the takeoff procedure is not alleviated without a suitable control strategy. The coaxial compound helicopter largely relies on nose-down and propeller propulsion for acceleration, limited by insufficient propulsive force from the rotor. Besides, the auxiliary propeller and the intensive interference between rotors complicate the flight dynamics of the vehicle. These factors underline the importance and difficulty of longitudinal control.

Time-frequency representations (TFRs) [30, 35] is introduced to reflect the temporal variations in a manoeuvre. For a control input time history, $\delta(t)$, the pilot time-varying cutoff frequency is given by $\omega_{co}(t)$, and the scalogram TFR of the stick power is given by $G_{\delta\delta}(\omega, t)$, which is relevant to the operation magnitude. There are periods with high time-varying cutoff frequencies, while the low stick activities have little or no practical consequence. Thus, time-varying power frequency, $G_\omega(t)$ is proposed as [35]

$$G_\omega(t_i) = \omega_{co}(t_i) \max G_{\delta\delta}(\omega, t_i) \tag{10}$$

which multiplies time-varying cutoff frequency by the maximum signal power at that instant t_i. As such, the power frequency is reduced whenever the pilot stick activity is low. Conversely, the power frequency is magnified whenever the pilot stick activity is high.

2.3.2 Sensitivity evaluation

The optimum distance varies with flight parameters. Hence, path sensitivity is proposed for aircraft safety, aiming at evaluating the possible deviation from the expected path due to flight parameter
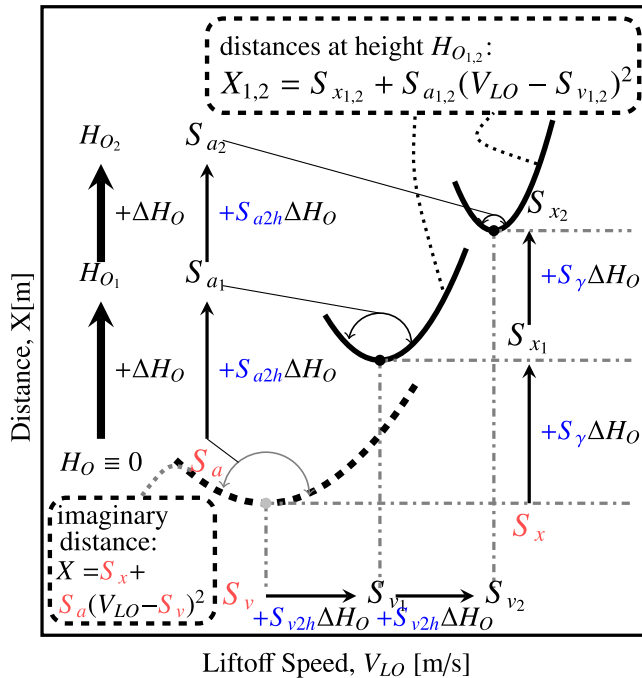
Figure 6. *Schematic diagram of sensitivity indices.*

variation. Although an optimal path is available in theoretical prediction, the actual trajectory might deviate from it due to pilot manoeuvre skills or environmental disturbance. In this case, the final distance might be much higher than the expected, resulting in obstacle contact. Therefore, a robust flight path is of vital importance for aircraft safety. In order to evaluate the robustness, the sensitivities of takeoff distance to liftoff speed, flight attitude, and obstacle height are analysed.

The takeoff distance could be expressed as a function of flight parameters according to the trajectory descriptions in Fig. 4(b). Based on the form of Equation (9a), the distance to a certain height is expressed as

$$X = \underbrace{(S_a + S_{a2h}H_O)}_{\text{related to acceleration}} \left(\left(V_{LO} - \underbrace{(S_v + S_{v2h}H_O)}_{\text{related to critical speed}}\right) \right)^2$$
$$+ S_x + \underbrace{S_\gamma H_O}_{\text{related to climb angle}} \tag{11}$$

where $S_{(\bullet)}$ are sensitivity indices. The schematic diagram (Fig. 6) shows the relationship between the six sensitivity indices, where two calculated paths (solid lines), denoted as X_1 and X_2, and an imaginary path (dotted line) at zero height are presented.

$(S_a + S_{a2h}H_O)$ represents the concavity of a quadratic curve, and refers to the distance variation to square of speed, i.e. is relevant to acceleration rate. It usually increases with height due to lift reduction as out of ground effect. $(S_v + S_{v2h}H_O)$ is related to the critical speed, V_{cL}, representing the speed for the minimum distance, $(S_x + S_\gamma H_O)$. Generally speaking, the critical speed increases with H_O [18] since high translational velocity benefits climbing. The last coefficient, S_γ, refers to the distance increment with obstacle height, and is relevant to the climbing angle.

The polynomial is a possible relationship between the distance and takeoff parameters, where high fitting coefficients indicates unpleasant deviation from the desired path. According to Fig. 6 and Equation (11), the sensitivities could be classified into three groups:
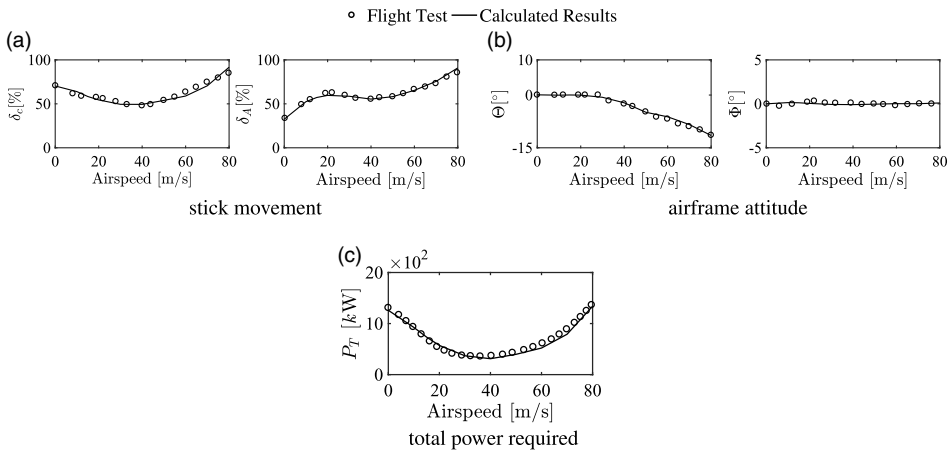
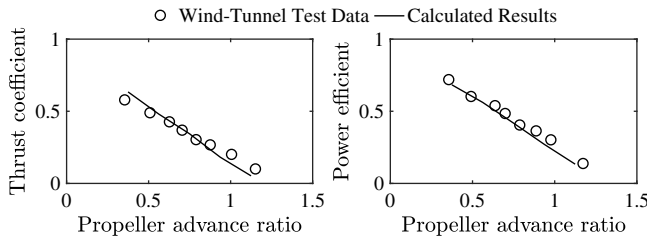**Figure 7.** *Level flight trim validation against flight test.*

Figure 8. *Low-speed propeller validation against wind tunnel test.*

1. baseline imaginary takeoff performance, including S_a, S_v and S_x
2. performance increment with obstacle height, including S_{a2h}, S_{v2h} and S_γ
3. total sensitivity at certain height, such as $S_a + S_{a2h}H_O$

3.0 Method validation and trim analysis

3.1 Model validation

In the coaxial compound helicopter, several key features influence the takeoff, such as the interference between rotors, rigid blades, and the propeller. In order to simulate these characteristics, a validated model is needed. Therefore, a rotorcraft with rich data published [8, 24, 29], XH-59A, is chosen as the prototype helicopter. Meanwhile, a propeller instead of the original propulsion is applied. The calculated stick movements, aircraft attitude and power required are validated against the flight test of the pure coaxial helicopter [8], as shown in Fig. 7. The large longitudinal stick movement at low speed indicates well-modelled interference between the coaxial rotors.

A propeller is applied to the coaxial compound helicopter, its parameters are the same as that in Ref. (2). The low-speed performance of the propeller is verified against wind-tunnel data [36]. The detail of the experimental eight-blade propeller settings and parameters can be found in Ref. (36). In propeller validation, the advancing ratio, lift and power coefficients are normalised by rotor rotation (rpm) and diameter. According to Fig. 8, the calculated results of the aircraft and propeller show good agreement with the flight test data.
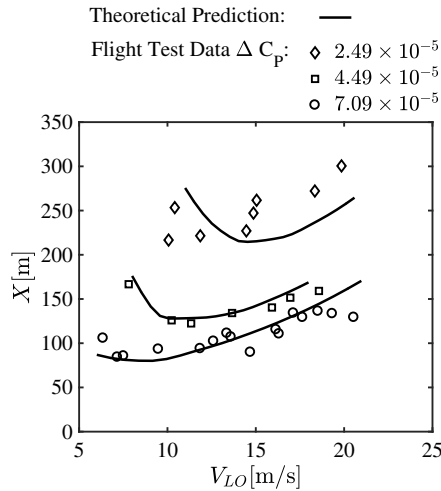
Figure 9. *Distance to clear a 50-ft obstacle, as a function of excess power and liftoff velocity.*

3.2 Method feasibility evaluation

For validation of the optimisation technique, the results generated by the theoretical model (solid curves) are compared against the flight test data of UH-1B [18]. Figure 9 shows the distance to clear a 50-ft obstacle as a function of liftoff speed for three excess power conditions. Detailed flight test operating parameters, such as gross weight, density altitude, and ambient temperature, are varied as per each power condition [18].

In Fig. 9, the optimal path model results show satisfying agreement with flight test data. In the two cases with relatively high excess power, the aircraft's takeoff procedure is similar to the ideal flight illustrated in Fig. 4. In other words, the acceleration and climbing ability is not degraded. By contrast, the theoretical predictions in the low-power case slightly underestimate the test results due to two factors. Firstly, the accuracy of the flight test data was influenced by integrated errors over a long takeoff time, especially in the heavily-loaded condition. The other reason is that the optimisation algorithm intends to search for the minimum distance to clear a given obstacle height, too ideal for realistic performance. After all, the theoretical model should be sufficient for predicting takeoff path and analysing relevant procedures.

3.3 Trim analysis

In the takeoff of a heavily loaded aircraft, the additional in-ground-effect (IGE) thrust benefits the acceleration. The influence of ground effect to level-flight trim power is presented in Fig. 10, with varying skid height and airspeed. The environmental air density altitude is assumed as 4,500m, atmospheric temperature as ISA + 15deg for simulating the heavily loaded condition. The takeoff weight is determined by the IGE hover with excess power for 0.5m/s climbing rate [37].

Figure 10(a) shows the total power required P_T as a function of skid height and forward flight speed with pure rotors without the propeller. The power gain from ground effect decreases as velocity or skid height increases, in line with the trend of ground effect. In the level flight trim of coaxial compound helicopter with turning propeller, the airframe attitude is preset to determine the propeller pitch [3, 7]. The power required at different pitch attitudes Θ and relevant gross weight are shown in Fig. 10(b). With similar excess power, there's no significant difference between their total power required. However, high attitude results in high propeller power (P_{pp}), leaving less power for rotor lift. As a result, the aircraft's maximum gross weight is degraded.

Table 1. *Flight parameters variation*

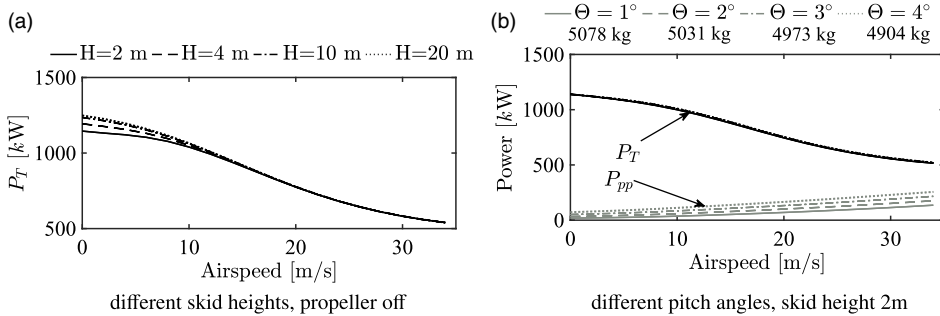| Flight parameters	Varying range
Minimum nose-down,Θ_{min}	$-5°$ and $-10°$
Obstacle height,H_O	7:5m, 10m, 15m and 20m
Liftoff speed,V_{LO}	5m/s to 15m/s

Figure 10. *Level flight trim power required of the aircraft.*

4.0 Propeller control design

A sequence of takeoff paths with different flight parameters are evaluated to control the propeller for global takeoff performance, as shown in Table 1. The minimum nose-down attitude in the level-flight phase is set as $-5°$ and $-10°$. Since a typical $10°$ nose-down generates an acceleration rate around $0.2g$ ($\tan(10°) \approx 0.18$), and fewer nose-down is required with extra propulsion. The obstacle height is set in a sequence of 7:5m, 10m, 15m and 20m, in line with that in Ref. (17).

According to the control link between the propeller and the rotor (in Equation (5)), the propeller pitch is determined by the hover state and the coefficient, K_{A2pp}. The trim analysis indicates the influence of attitude to gross weight. Thus, the feasibility of designing a controller without degrading maximum takeoff weight is studied first.

4.1 Initial propeller thrust design

The influence of airframe attitude on takeoff distance is presented in Figs 11 and 12. Different flight parameters are considered for an overall evaluation. The slices at certain attitude and liftoff speeds are also given. The coefficient K_{A2pp} is assumed as an optimisation parameter to exclude its influence, and the optimised results are given in Fig. 13.

According to the three figures, the initial pitch angle for takeoff is set as $1°$ for three reasons. Firstly, as discussed in the trim analysis (Fig. 10(b)), the aircraft is of heavier gross weight with a lower pitch angle. In this case, the controller designed for a severe condition is compatible with a lighter aircraft. The second factor is relevant to the distance. According to Figs 11(b) and 12(b), the distances show a near-linear trend with attitude. It indicates that the distance reduction is caused by the light weight other than the initial propulsion. In other words, despite the heavier weight, the takeoff distance is hardly degraded by the attitude, especially as liftoff speed increases. Although there is a sharp rise at low speeds, it is avoidable by performing a short takeoff. Thus, it is feasible to introduce the propeller while maintaining the vehicle's maximum gross weight. Last but not least, low initial propulsion benefits the following operation, as indicated by Fig. 13. The case of $\Theta_{ini} = 1°$ has the broadest positive range and smallest variation of the K_{A2pp}. Thus, the designed controller would not be too far from the optimum. On the contrary, a high attitude limits the propeller pitch increment, resulting in reverse propulsion increment from the rotors and propeller.
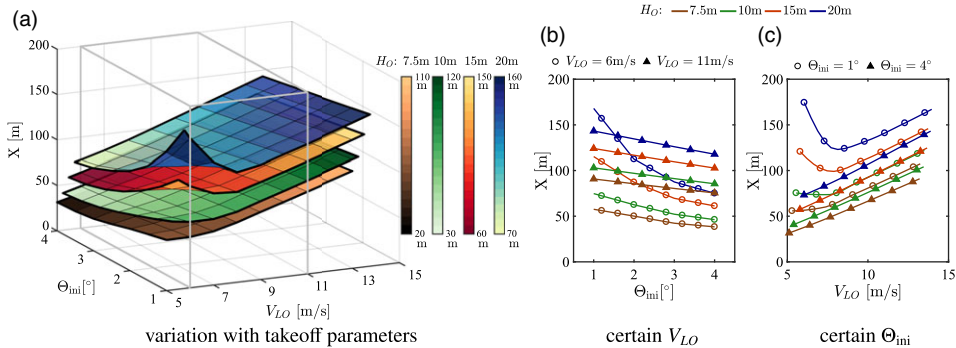
Figure 11. *Takeoff distances under different airframe pitch angles $\Theta_{\min} = -5°$.*
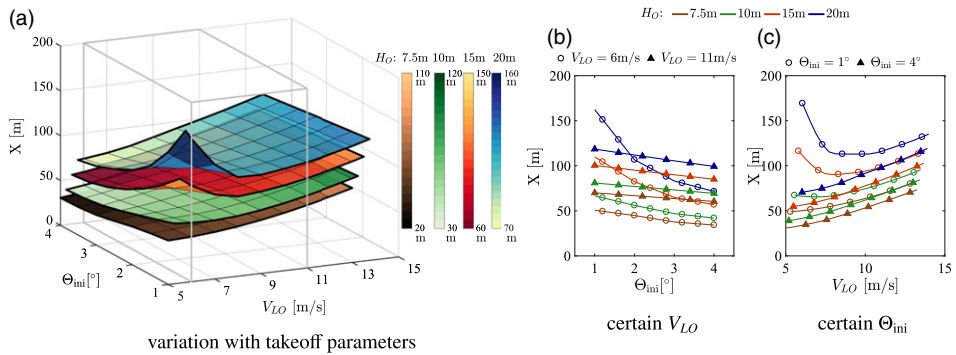

Figure 12. *Takeoff distances under different airframe pitch angles $\Theta_{\min} = -10°$.*
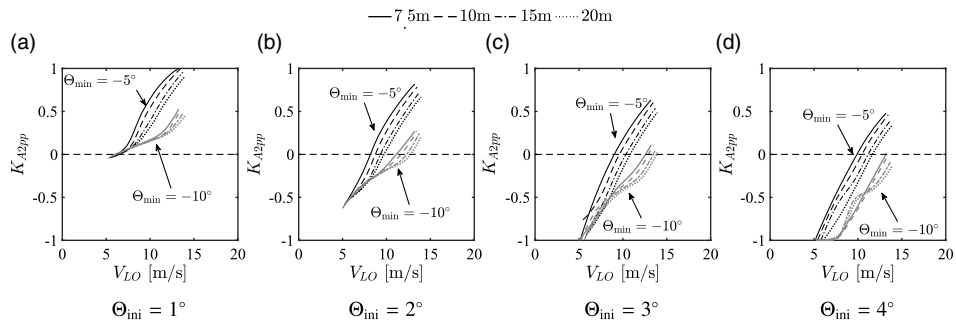

Figure 13. *Optimal allocation variation with takeoff parameters under different initial pitch angles.*

The distribution of K_{A2pp}, shown in Fig. 13, reflects the best allocation variation with takeoff parameters. These curves could be classified into two groups by the attitude constraint. The group of $\Theta_{\min} = -5°$ is higher, where high K_{A2pp} makes up the level acceleration. In each group, K_{A2pp} increases with liftoff speed for better acceleration, decreasing with obstacle height for more climbing power. To sum up, the allocation shows a regular trend with flight parameters, with minor variations. In addition, there is a high coincidence at low speed, indicating the feasibility of a constant allocation.
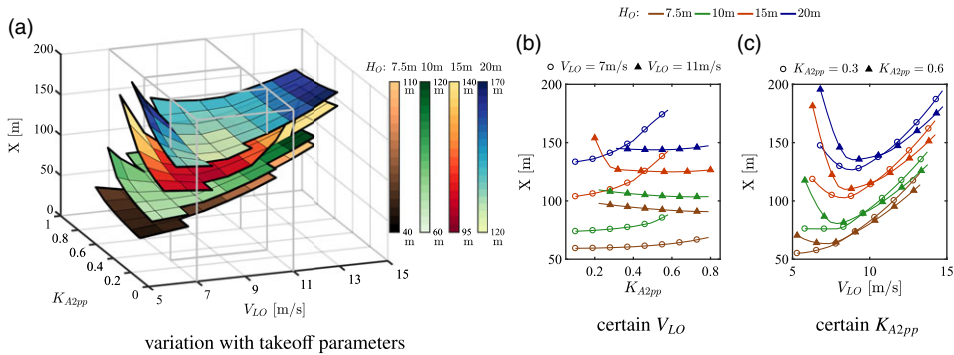
Figure 14. *Takeoff distances under different airframe pitch angles* $\Theta_{\min} = -5°$.
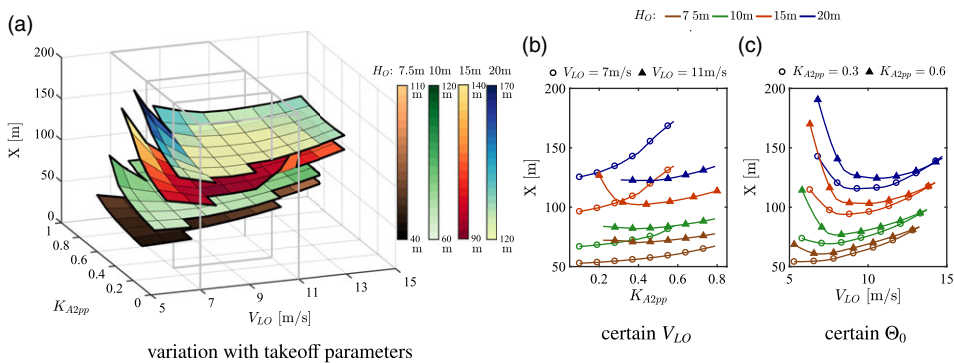

Figure 15. *Takeoff distances under different airframe pitch angles* $\Theta_{\min} = -10°$.

4.2 Control allocation design

In this subsection, a constant allocation for global takeoff performance is designed. In order to avoid reverse propulsion from the propeller and rotor that significantly damages the rotorcraft's handling quality, a positive K_{A2pp} is preferred. Its influence on paths is calculated and evaluated, with K_{A2pp} from 0.1 to 0.8 at an interval of 0.1.

4.2.1 Takeoff distance

The distances under different allocations are presented in Figs 14 and 15, with varying takeoff parameters. There are infeasible solutions and steep rises when the allocation is below 0.3 or above 0.6. Too low K_{A2pp} results in a low propeller pitch increment as translational velocity increases, and a high K_{A2pp} leads to insufficient power for climbing. In the cases between 0.3 and 0.6, low allocation usually achieves significantly shorter distances, especially at low liftoff speeds. According to Fig. 13, a high allocation is preferred at high velocity. By contrast, the length is slightly shortened or even longer according to the Figs 14(b), (c) and 15(b), (c). Therefore, a low coefficient is preferred from aspects of distance. Nevertheless, the range of 0.3–0.6 is chosen for an overall path evaluation on pilot workload and sensitivities.

4.2.2 Pilot workload analysis

The power frequencies of the stick movements under different K_{A2pp} are shown in Figs 16 and 17. The obstacle height and relevant speeds are given in each subfigure, with speed increment of 2m/s. There is
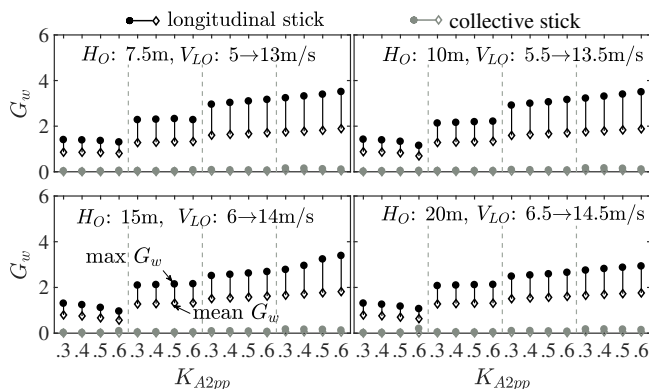
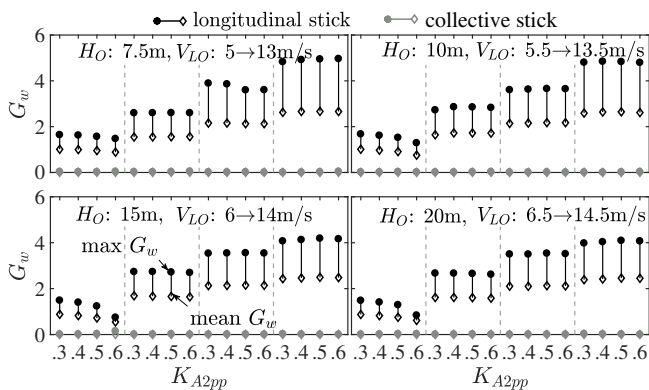**Figure 16.** *Pilot workload under different allocations* $\Theta_{\min} = -5°$.

Figure 17. *Pilot workload under different allocations* $\Theta_{\min} = -10°$.

hardly any collective movement, resulting from two reasons. Firstly, pulling up the collective stick with little excess power is not practical. On the other hand, lowering the stick increases the pilot operation and degrades climbing. Thus, the collective is held constant. The longitudinal power frequency varies with fight paths. It rises with height or as pitch constraint from $-5°$ to $-10°$, where more longitudinal operations are needed. Nevertheless, the pilot workload hardly changes with the allocation. In other words, although the allocation influences flight paths and operations with different propulsion, the range of power frequencies (multiplication of frequency by stick movement) are similar. Thus, the recommended allocation range is still between 0.3 and 0.6.

4.2.3 Sensitivity analysis

Table 2 presents the distance sensitivity indices under different allocations when $\Theta_{\min} = -5°$, which are numerical representations of the distance variation in Fig. 14. The indices, S_a and S_{a2h}, represent the overall trend of paths against speed. Their rapid increases with allocation are in line with the steep rises at high K_{A2pp} and high height. Thus, the low allocation has the lowest acceleration sensitivities for all heights. S_v refers to the imaginary critical speed at zero obstacle height. It is the lowest when $K_{A2pp} = 0.3$ because of more excess power from low propulsion. The critical speed increment with height is presented by S_{v2h}. Despite the lowest S_{v2h} of high allocation (0.6), its critical speed ($V_{cL} = S_v + S_{v2h}H_O$) is the highest for all heights. As a result, the level acceleration path, represented by S_x, is longer. Although the lower S_γ partially offsets its distance disadvantage as height increases, the total distance remains the longest. Therefore, the high allocation has high sensitivities despite the minor alleviation as height increases.

Table 2. *Distance sensitivity under different allocations* $\Theta_{\min} = -5°$

K_{A2pp}	S_a	S_{a2h}	S_v	S_{v2h}	S_x	S_γ
0.3	0.687	0.063	3.51	0.27	14.89	6.00
0.4	0.695	0.075	4.22	0.26	18.61	5.93
0.5	0.732	0.103	5.27	0.25	23.45	5.77
0.6	0.764	0.164	6.72	0.21	30.56	5.31

Table 3. *Distance sensitivity under different allocations* $\Theta_{\min} = -10°$

K_{A2pp}	S_a	S_{a2h}	S_v	S_{v2h}	S_x	S_γ
0.3	0.257	0.067	5.05	0.27	20.73	4.83
0.4	0.210	0.083	5.69	0.26	23.51	4.75
0.5	0.005	0.128	6.71	0.23	27.64	4.53
0.6	−0.135	0.165	8.01	0.19	33.62	4.23

The sensitivities when $\Theta_{\min} = -10°$ are shown in Table 3. Their trends with K_{A2pp} are similar to the corresponding cases in Table 2, except the rapid decrease of acceleration indicator S_a. The negative S_a in the high-allocation case indicates the narrowed gap of acceleration sensitivities with the others. However, it remains the highest at all heights. From $\Theta_{\min} = -5°$ to $-10°$, there are no significantly numerical changes in height-related sensitivities, such as S_{a2h} and S_{v2h}. Because climbing ability largely depends upon liftoff speed for climbing power other than nose-down attitude. Hence, high allocation still has the highest sensitivities.

Finally, the proposed K_{A2pp} for the coaxial compound helicopter is set as 0.3. Its takeoff distance is relatively the shortest among all allocations, as demonstrated in the distance discussion and relevant sensitivity indices (S_x,S_γ). In addition, its acceleration- and speed-related sensitivities at all heights are the lowest. Although the increments with height, S_{v2h} and S_γ, are slightly higher, the minor increases are acceptable considering the magnitude of speed and distance.

4.3 Assessment of the proposed controller

From the research above, the combination of low attitude (1°) and moderate allocation (K_{A2pp}) achieves the best takeoff performance among all cases. Here, a baseline strategy is introduced for assessing the proposed controller. Only the rotor is operated in the baseline, and the propeller is not engaged. The takeoff paths under the two strategies are calculated with the aircraft under the same gross weight and atmospheric conditions.

The distances under the two propeller control strategies are given in Fig. 18. According to the imaginary distances at $H_O = 0$, the propeller control benefits the level acceleration. As a result, the proposed strategy (triangle symbols) requires fewer distances to the same height in all cases, with the average length shortened by 12.6%.

From Fig. 19, the longitudinal pilot workload is lower than the baseline. The mean power frequency is reduced by 9.8% on average, and the maximum by 7.3%. Higher alleviation is obtained in the cases of higher liftoff speed, height or nose-down, where longer acceleration is required. It is because the propulsion alleviates stick movement for acceleration.

The sensitivity indices under different strategies are presented in Table 4, with varying attitudes. Almost all indicators are significantly alleviated by applying the proposed method, indicating the path is less sensitive to liftoff speed or height deviation. Also, the distance is shorter, in line with results from Fig. 18. In addition, the path deviation caused by different attitudes is reduced, as shown by the narrowed gaps between cases of $-5°$ and $-10°$. Therefore, the takeoff path sensitivities to all three flight parameters are fully alleviated.

Table 4. *Distance sensitivity comparison between the proposed and baseline strategies*

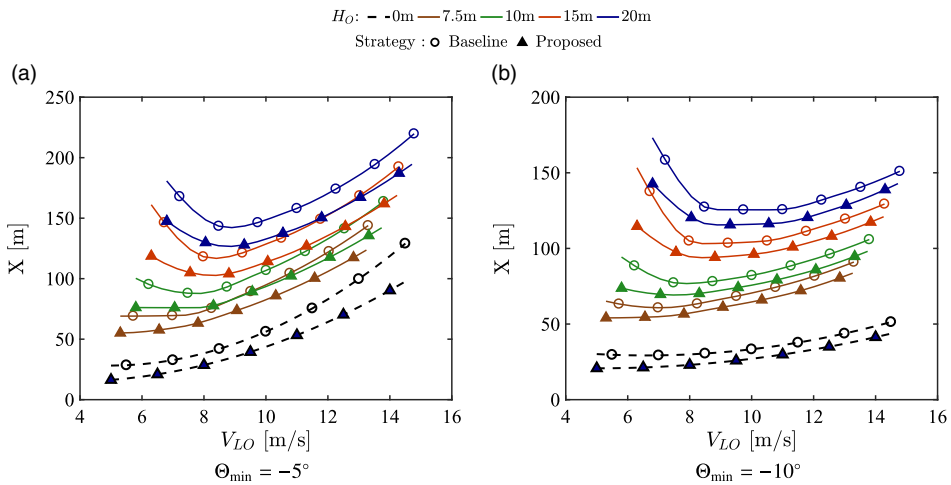| Strategy	Θ_{min}	S_a	S_{a2h}	S_v	S_{v2h}	S_x	S_γ
Baseline	$-5°$	1.11	0.09	4.98	0.23	28.16	6.28
	$-10°$	0.35	0.107	6.60	0.22	29.23	4.77
Proposed	$-5°$	0.69	0.063	3.51	0.27	14.89	6.00
	$-10°$	0.26	0.067	5.05	0.27	20.73	4.83

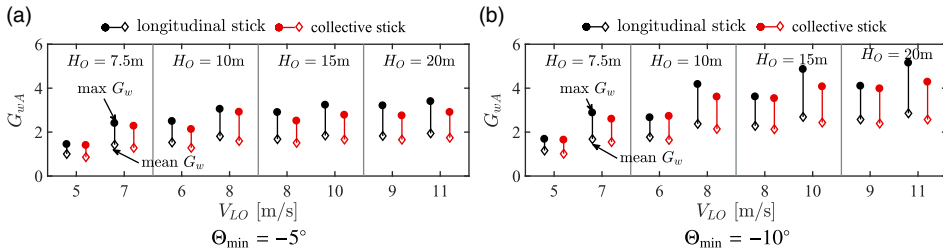**Figure 18.** *Takeoff distance comparison between the proposed and baseline strategies.*

Figure 19. *Longitudinal pilot workload comparison between the proposed and baseline strategies.*

In practice, the non-rotating propeller would produce additional drag, which is neglected in this paper. Thus, it can be foreseen that the performance in real scenarios should be further worse than the baseline calculation results. On the other hand, the propeller effects are considered in this propeller-embedded optimisation. Meanwhile, the results indicate that its performance, including takeoff distance, pilot workload, and sensitivity, is significantly improved even compared to the baseline calculation results. This outcome demonstrates that it is feasible and helpful to integrate the propeller into the low-speed takeoff.

5.0 Conclusions

This work investigates the propeller control to enhance the global takeoff performance of a heavily loaded coaxial compound helicopter. The takeoff performance is evaluated from three aspects, distance, pilot workload and proposed path sensitivity regarding flight parameters. In this work, the trend of

distance to liftoff speed, nose-down attitude and flight height are quantified by six path sensitivity coefficients. Then the six quantities are applied to develop takeoff technique of high robustness to flight procedure.

The propeller control design includes two aspects, the initial propulsion at hover state and the rotor-propeller linkage throughout the takeoff procedure. In terms of the initial state, a low propeller thrust at hover is recommended to improve takeoff performance while maintaining the aircraft's maximum gross weight. By contrast, high initial propulsion degrades the coupling operation of the propeller and rotor. Meanwhile, a moderate control allocation on the propeller is preferred, which results in the shortest takeoff distance. Either high or low allocation can lead to sharp increases in length or even infeasible solutions. In addition, high propeller pitch increments result in high path sensitivity to takeoff speed, flight attitude, and obstacle height. In other words, a potentially large deviation from the expected path.

By applying the proposed propeller control, the takeoff performance of the aircraft is improved significantly compared to pure rotor flight. The average distance is shortened by 12.6%. The mean and maximum longitudinal power frequencies, representing the pilot workload, are reduced by an average of 9.8% and 7.3%. Furthermore, lower path sensitivities to takeoff parameters are achieved.

References

[1] Foote, B.C., Kaye, J.A., Weintraub, A.Q. et al. Speed and maneuverability benefits of Sikorsky's X2 Technology™ versus air-defense artillery, In *Vertical Flight Society 75th Annual Forum & Technology Display*. AHS International, Philadelphia, PA, USA, 2019, p 6.

[2] Yuan, Y., Thomson, D. and Chen, R. Variable rotor speed strategy for coaxial compound helicopters with lift–offset rotors, *Aeronaut J*, 2020, **124**, (1271), pp 96–120.

[3] Yuan, Y., Thomson, D. and Chen, R. Propeller control strategy for coaxial compound helicopters, *Proc Inst Mech Eng G J Aerosp Eng*, 2019, **233**, (10), pp 3775–3789. http://journals.sagepub.com/doi/10.1177/0954410018806796

[4] Walsh, D., Weiner, S., Arifian, K. et al. High airspeed testing of the Sikorsky X2 Technology Demonstrator, In *American Helicopter Society 67th Annual Forum*. AHS International, Virginia Beach, VA, 2011, pp 2999–3010.

[5] Yuan, Y., Chen, R. and Thomson, D. Propeller design to improve flight dynamics features and performance for coaxial compound helicopters, *Aerosp Sci Technol*, 2020, **106**, p 106096. https://linkinghub.elsevier.com/retrieve/pii/S1270963820307781

[6] Ferguson, K. and Thomson, D. Flight dynamics investigation of compound helicopter configurations, *J Aircr*, 2015, **52**, (1), pp 156–167. http://arc.aiaa.org/doi/10.2514/1.C032657

[7] Ferguson, M.K. *Towards a better understanding of the flight mechanics of compound helicopter configurations*, PhD Thesis, University of Glasgow, Glasgow, Scotland, UK, 2015.

[8] Ruddell, A.J. Advancing Blade Concept (ABCTM) Development, Technical Report USAAVRADCOM-TR-81-D-5, Sikorsky Aircraft Division of United Technologies Corporation, 1981.

[9] Ruddell, A. Advancing blade concept (ABC) development test program. In *1st Flight Test Conference*. American Institute of Aeronautics and Astronautics, Las Vegas, NV, USA, 1981, p 2437. http://arc.aiaa.org/doi/10.2514/6.1981-2437

[10] Xin, H., Zhang, C., Black, A. et al., S-97 Raider® GENHEL Model development and correlation with flight test data, In *Vertical Flight Society (VFS) 77th Annual Forum & Technology Display*. AHS International, Virtual Event, 2021, p 13.

[11] Walsh, D., Weiner, S., Arifian, K. et al. Development testing of the Sikorsky X2 Technology Demonstrator, In *American Helicopter Society 65th Annual Forum*. AHS International, Grapevine, Texas, 2009, pp 1–11.

[12] Hall, C., Zachariadis, A., Brandvik, T. et al. How to improve open rotor aerodynamics at cruise and take-off. *Aeronaut J*, 2014, **118**, (1208), pp 1103–1123.

[13] Qian, F., Strusevich, V., Gribkovskaia, I. et al. Minimization of passenger takeoff and landing risk in offshore helicopter transportation: Models, approaches and analysis, *Omega*, 2015, **51**, pp 93–106. https://linkinghub.elsevier.com/retrieve/pii/S0305048314001030

[14] Zhao, Y., Jhemi, A.A. and Chen, R.T.N. Optimal vertical takeoff and landing helicopter operation in one engine failure. *J Aircr*, 1996, **33**, (2), pp 337–346. https://arc.aiaa.org/doi/10.2514/3.46943

[15] Bibik, P. and Narkiewicz, J. Helicopter optimal control after power failure using comprehensive dynamic model, *J Guidance, Control Dyn*, 2012, **35**, (4), pp 1354–1362. https://arc.aiaa.org/doi/10.2514/1.51371

[16] Enciu, K. and Rosen, A. Safety considerations for helicopter roll on takeoffs. *J Aircr*, 2011, **48**, (3), pp 952–962. https://arc.aiaa.org/doi/10.2514/1.C031183

[17] Schmitz, F. and Rande Vause, C. A simple, near-optimal takeoff control policy for a heavily loaded helicopter operating from a restricted area, In *Mechanics and Control of Flight Conference*. American Institute of Aeronautics and Astronautics, Anaheim, CA, USA, 1974, pp 1–8. http://arc.aiaa.org/doi/10.2514/6.1974-812

[18] Schmitz, F.H. and Vause, C.R. Near-optimal takeoff policy for heavily loaded helicopters exiting from confined areas, *J Aircr*, 1976, **13**, (5), pp 343–348. https://arc.aiaa.org/doi/10.2514/3.58666

[19] Thomson, D., Taylor, C., Talbot, N. et al. Investigation of piloting strategies for engine failures during takeoff from offshore platforms, *Aeronaut J*, 1995, **99**, pp 15–25.

[20] Carlson, E.B. *Optimal Tiltrotor Aircraft Operations during Power Failure*, PhD Thesis, University of Minnesota, Minnesota, USA, 1999. http://adsabs.harvard.edu/abs/1999PhDT.......225C

[21] Enciu, K. and Rosen, A. Helicopter roll-on takeoff simulation, *J Am Helicopter Soc*, 2011, **56**, (1), pp 12003–12015.

[22] Weiand, P. and Krenik, A. A multi-disciplinary toolbox for rotorcraft design, *Aeronaut J*, 2018, **122**, (1250), pp 620–645.

[23] Johnson, W. NDARC NASA Design and Analysis of Rotorcraft, Technical Publication NASA/TP—2015–218751, NASA, 2015.

[24] Valkov, T. Aerodynamic loads computation on coaxial hingeless helicopter rotors. In *28th Aerospace Sciences Meeting*, volume AIAA 90-0070. Montreal, Canada: American Institute of Aeronautics and Astronautics, 1990, p 14. https://arc.aiaa.org/doi/abs/10.2514/6.1990-70

[25] Zhao, Y., Yu, X. and Chen, R. Height-Velocity Characteristics Comparisons of Single-rotor and Coaxial Helicopters. In *Vertical Flight Society (VFS) 77th Annual Forum & Technology Display*. AHS International, Virtual Event, 2021, p 12.

[26] Cheeseman, I.C. and Bennett, W. The Effect of the Ground on a Helicopter Rotor in Forward Flight, Reports and Memoranda R&M. No. 3021, Aeronautical Research Council, London, 1955.

[27] Lim, J.W., McAlister, K.W. and Johnson, W. Hover performance correlation for full-scale and model-scale coaxial rotors. *J Am Helicopter Soc*, 2009, **54**, (3), pp 32005–32014. http://www.ingentaconnect.com/content/10.4050/JAHS.54.032005

[28] Tr, A. Performance and loads data from a wind tunnel test of a full-scale, coaxial, hingeless rotor helicopter. Technical Memorandum NASA-TM-81329, Ames Research Center, 1981.

[29] Pleasants, W.A. A rotor technology assessment of the advancing blade concept. Technical Memorandum NASA-TM-84298, Ames Research Center, 1983.

[30] Yan, X. and Chen, R. Augmented flight dynamics model for pilot workload evaluation in tilt-rotor aircraft optimal landing procedure after one engine failure. *Chin J Aeronaut*, 2019, **32**, (1), pp 92–103. https://doi.org/10.1016/j.cja.2018.06.010

[31] Bottasso, C.L., Maisano, G. and Scorcelletti, F. Trajectory optimization procedures for rotorcraft vehicles including pilot models, with applications to ADS-33 MTEs, cat-a and engine off landings. In *American Helicopter Society 65th Annual Forum*, AHS International, 2009, p 15.

[32] Yu, Z., Yan, X. and Chen, R. Prediction of pilot workload in helicopter landing after one engine failure. *Chin J Aeronaut*, 2020, **33**, (12), pp 3112–3124. https://linkinghub.elsevier.com/retrieve/pii/S100093612030248X

[33] Sharma, V. Optimal Category-A Helicopter Flight Trajectories for Operation from a Clear Heliport, Technical report, Ames Research Center, 1995. https://ntrs.nasa.gov/search.jsp?R=20020011642

[34] Chi, C., Yan, X., Chen, R. et al. Analysis of low-speed height-velocity diagram of a variable-speed-rotor helicopter in one-engine-failure. *Aerosp Sci Technol*, 2019, **91**, pp 310–320. https://doi.org/10.1016/j.ast.2019.05.003

[35] Tritschler, J.K., O'Connor, J.C., Klyde, D.H. et al. Analysis of pilot control activity in ADS-33e mission task elements, In *American Helicopter Society 72th Annual Forum*. AHS International, 2016, pp 150–174.

[36] Dunham, D.M., Gentry, J.G.L. and Coe, Jr, P.L. Low-speed wind-tunnel tests of single- and counter-rotation propellers, Technical Memorandum NASA-TM-87656, NASA Langley Research Center Hampton, 1986. https://ntrs.nasa.gov/citations/19860013081

[37] Federal Aviation Administration. *Advisory Circular 29-2C, Certification of Transport Category Rotorcraft*, 2008.